

# Revisiting the double-well problem by deep learning with a hybrid network

Shurui Li<sup>1</sup>, Jianqin Xu<sup>1</sup>, and Jing Qian<sup>1,\*</sup>

<sup>1</sup>Department of Physics, School of Physics and Electronic Science, East China Normal University, Shanghai 200062, China

\*corresponding: jqian1982@gmail.com

## ABSTRACT

Solving physical problems by deep learning is accurate and efficient mainly accounting for the use of an elaborate neural network. We propose a novel hybrid network which integrates two different kinds of neural networks: LSTM and ResNet, in order to overcome the difficulty met in solving strongly-oscillating dynamics of the system's time evolution. By taking the double-well model as an example we show that our new method can benefit from a pre-learning and verification of the periodicity of frequency by using the LSTM network, simultaneously making a high-fidelity prediction about the whole dynamics of system with ResNet, which is impossibly achieved in the case of single network. Such a hybrid network can be applied for solving cooperative dynamics in a system with fast spatial or temporal modulations, promising for realistic oscillation calculations under experimental conditions.

## Introduction

Deep learning (DL) has been devoted to solving physical problems in recent years. Depending on its powerful ability to make predictions about data and to extract meaningful features, exciting progresses have been made in the fields of quantum dynamics<sup>1,2</sup>, many-body physics<sup>3</sup>, precision measurement<sup>4</sup>, condensed-matter physics<sup>5-9</sup> and quantum machine learning<sup>10-12</sup>. When applying DL we will face the primary problem of establishing a suitable network, in which the data set could be efficiently trained with the network. So far several neural networks are utilized. For example, the earlier artificial neural network can approximate any distributions with only two neural layers<sup>13</sup>; but it is inaccurate when the layer number is increased<sup>14</sup>. The restricted Boltzmann machine is an unsupervised method, which can uncover the information underlying the data by learning the joint distribution with Bayesian theory<sup>15</sup> yet it is difficult to train the system without a fine partition-function solution<sup>16</sup>. Other neural network(NN)s like convolutional NN<sup>17</sup> or recurrent NN<sup>18</sup> are more universal in extracting local features of data and learning the relationship between elements with high accuracy<sup>19,20</sup>, despite they may face the problem of gradient exploding or gradient vanishing due to the complexity of dynamics. Therefore a single type of neural network becomes incapable of solving complex population dynamics.

In parallel simulating a system with fast oscillations usually depends on the precision of sampling interval<sup>21</sup>. When the sampling interval is insufficient numerical ways may arise poor outcomes that are largely deviated from its real numbers<sup>22</sup>. However a high-precision sampling adds to the cost of experiment; in theory it also leads to a long-time calculation limited by the computer capacity. Therefore it is quite difficult to accurately obtain the fast-oscillating dynamics both in theory and experiment. In the present work we propose a hybrid neural network involving two different networks which are so-called Long short-term memory(LSTM)<sup>23</sup> and Residual network(ResNet)<sup>24,25</sup>, in order to study the population dynamics of a system's evolution. Taking a generalized double-well system as an example, we show that the modified DL method can perfectly solve the imbalanced population evolution between two wells and represent the behaviors of population, phase and frequency with high fidelity. The double-well optical potential serving as a basic platform for studying population dynamics, has been widely investigated with fermions<sup>26</sup>, ultracold bosons<sup>27</sup>, atomic Bose-Einstein condensates(BECs)<sup>28</sup>, *etc.*

As for the atomic BECs trapped in a double-well system a large number of achievements were carried out arising a well-solved theory<sup>29-31</sup>. This fact provides us with an easier generation of enough training datum via the Runge-Kutta method beforehand. Our hybrid network enables a highly-efficient learning of frequency based on the periodicity verification of strongly-oscillating dynamics. Moreover even if the original datum is not enough the LSTM network can perform a reliable prediction about higher frequency values on the macroscopic quantum self-trapping (MQST) regime, which are far beyond the trained parameters. However we note that the numerical method fails to work in this case because of the inadequate sampling. Compared to the direct learning involving single neural network, integrating LSTM and ResNet can deeply increase the learning efficiency despite expending a slightly longer training time due to more layers needed for constructing two networks.

The final infidelity obtained by estimating the deviation of fractional population difference can be much lower than 0.01 with the help of hybrid network learning.

## Double-well Theory

A double-well model serving as a basic platform in the study of microscopic mediums, especially for atomic BECs<sup>32–36</sup>, has been focused by researchers for decades. A typical double-well potential can be easily created by a combination of periodic optical potential with a strong harmonic confinement played by a periodic one-dimensional light shift<sup>37</sup>. If two atomic condensates are confined in such a double-well optical trap, the effects of boson Josephson junction (BJJ) or MQST can be observed.

Our study starts from a brief introduction of double-well theory in which the wave function  $\psi(x, t)$  of two weakly-linked atomic condensates is expanded as

$$\psi(x, t) = a_1(t)\phi_1(r) + a_2(t)\phi_2(r). \quad (1)$$

under the mean-field approximation. To be universal we consider two wells are asymmetric and set an energy difference  $\gamma$  between them. A standard treatment for the population dynamics in two wells can be expressed as (here  $\hbar = 1$ )

$$i \frac{d}{dt} \begin{pmatrix} a_1 \\ a_2 \end{pmatrix} = \hat{H} \begin{pmatrix} a_1 \\ a_2 \end{pmatrix} \quad (2)$$

with the Hamiltonian  $\hat{H}$  given by

$$\hat{H} = \begin{pmatrix} \gamma + U_1 N_1 & -K \\ -K & U_2 N_2 \end{pmatrix} \quad (3)$$

and the amplitudes  $a_j = \sqrt{N_j} e^{i\theta_j}$  with  $N_j$ ,  $\theta_j$  the number and phase of particles in trap  $j \in (1, 2)$ . Here one keeps  $N_T = N_1 + N_2$  a constant and  $U_j$  is the trapped atomic interaction which is related to the atomic scattering length.  $K$  is the inter-trap coupling coefficient<sup>29</sup>. Upon defining the phase difference  $\phi = \theta_2 - \theta_1$  and the fractional population difference  $z = \frac{N_1 - N_2}{N_T}$ , equation (2) can be re-organized as

$$\begin{aligned} \dot{z}(t) &= -\sqrt{1 - z^2(t)} \sin[\phi(t)], \\ \dot{\phi}(t) &= \Delta E + \Lambda z(t) + \frac{z(t)}{\sqrt{1 - z^2(t)}} \cos[\phi(t)], \end{aligned} \quad (4)$$

in which we rescale the time by  $2Kt \rightarrow t$  ( $2K$  is the frequency unit) and other dimensionless parameters are

$$\begin{aligned} \Delta E &= \gamma/2K + (U_1 - U_2)N_T/4K, \\ \Lambda &= (U_1 + U_2)N_T/4K. \end{aligned} \quad (5)$$

accordingly, which indicate the imbalanced energy as well as the atomic tunneling rate. Solving  $z(t)$  and  $\phi(t)$  in equation (4) essentially gives rise to the entire population dynamics in double-well system.

It is clearly shown that the pair of variables  $z(t)$  and  $\phi(t)$  are canonically conjugate satisfying  $\dot{z} = -\frac{\partial H}{\partial \phi}$ ,  $\dot{\phi} = \frac{\partial H}{\partial z}$ . Based on that the Hamiltonian  $\hat{H}$  can be rewritten as

$$\hat{H} = \frac{\Lambda}{2} z^2 + \Delta E z - \sqrt{1 - z^2} \cos \phi, \quad (6)$$

By simply assuming  $\gamma = 0$  (symmetric trap) and ensuring  $U_1 = U_2 = U$ , it leads to  $\Delta E = 0$ ,  $\Lambda = UN_T/2K$ . The initial energy starts from

$$H_0 = \frac{\Lambda}{2} z(0)^2 - \sqrt{1 - z(0)^2} \cos \phi(0), \quad (7)$$

which is conserved during the dynamical evolution. According to the initial phase difference  $\phi(0) = 0$  or  $\pi$  we can obtain the zero-mode or  $\pi$ -phase mode individually, and we focus on the former here.  $z(0) \in [-1, 1]$  stands for the initial population imbalance and is tunable. In experiment via the adjustment of  $\Lambda \sim U/K$  that characterizes the relative strength between interaction and tunneling rate of two wells we can observe two regimes: BJJ and MQST. The former meets  $\langle z(t) \rangle = 0$  and  $\langle \phi(t) \rangle = 0$  around  $z = 0$  when  $\Lambda$  is small. As increasing  $\Lambda$  that exceeds a critical value  $\Lambda_c$ , the population oscillation becomes self-trapped giving to  $\langle z(t) \rangle \neq 0$  on average. This behavior is also accompanied by an unbound and increasing phase that is winding with time.

The critical value between Josephson oscillation and self-trapping effects has been analytically solved at  $H_0 = 1$ , arising<sup>28</sup>:

$$\Lambda_c = \frac{2 + 2\sqrt{1 - z(0)^2} \cos \phi(0)}{z(0)^2} \quad (8)$$

which means if the initial energy increases exceeding  $H_0 = 1$  the fractional population difference will reveal a significant change, corresponding to the critical point between two regimes.

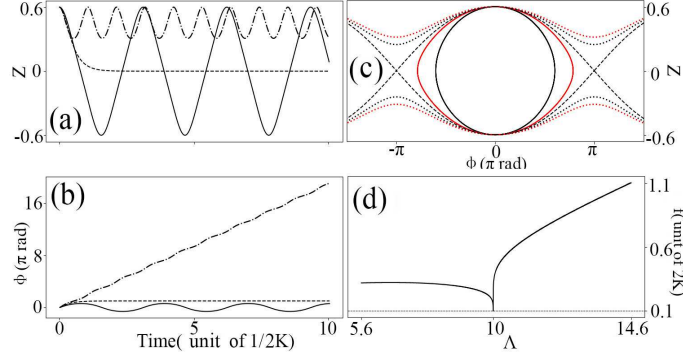


**Figure 1.** (a-b) Numerical results  $z(t)$  and  $\phi(t)$  obtained by solving equation (4) with the Runge-Kutta method for  $\Lambda = 6.2$ (solid), 10(dashed, critical value) and 13.4(dash-dotted). (c) The  $(z - \phi)$  diagram under  $\Lambda = 6.2$ (black solid), 8.8(red solid), 10(black-dashed), 11.8(red-dotted), 13.4(black-dotted). (d) Oscillating frequency  $f$  of  $z(t)$  for  $\Lambda \in [5.6, 14.6]$ . At the critical point  $\Lambda_c = 10$ , we set  $f = 0.1$ .

Our numerical simulations for solving  $z(t)$  and  $\phi(t)$  based on a standard fourth-order Runge-Kutta method, are explicitly presented in Fig.1(a-b). As expected, both population oscillation and phase variation manifest a significant transition across the critical value  $\Lambda_c$ . If  $\Lambda < \Lambda_c$  a BJJ appears between two wells accompanied by a small phase fluctuation in time, ensuring  $\langle z(t) \rangle = \langle \phi(t) \rangle = 0$ . However when  $\Lambda$  becomes larger the population tends to be self-trapped in one well with a time-dependent and increasing phase. Figure 1(c-d) show a global representation of phase diagram in the  $(z, \phi)$  space as well as the oscillating frequency  $f$  versus  $\Lambda$ . The critical transition at  $\Lambda_c = 10$  is clearly seen, agreeing with the discussions in (a-b). These numerical results provide us with a sufficient and accurate data set to train the network. The DL method, not only can be regarded as a certification for the numerical results; but also enables a prediction about unknown results which are beyond the test parameter range.

## Direct Learning

For showing the robustness of DL that can be applied for physical problems we aim to solve the fractional population difference and phase dynamics in a double-well trap, simply using this method. Nowadays DL can be regarded as a shortcut for this target. Because once a data set has been formed by original numerical solutions, *e.g.* in the current case, it reveals its strength in generating similar results for  $\phi(t)$  and  $z(t)$  with the trained network. Most interestingly, it can even predict about unknown results beyond the original data set with the strong prediction ability.

Our work starts from equation (4) by setting *e.g.*  $z(0) = 0.6$ ,  $\phi(0) = 0$ , arising  $\Lambda_c = 10$ . The original parameter is fixed to  $\Lambda \in [5.6, 14.6]$  covering two regimes. The data set is formed by uniformly separating 90001  $\Lambda$  values within  $\Lambda \in [5.6, 14.6]$ , and solving the corresponding  $\phi(t)$  and  $z(t)$  for each  $\Lambda$  via the method of fourth-order Runge-Kutta algorithm. The time interval is  $\Delta t = 0.02$  with a unit of  $1/2K$ . As a result, we finally obtain two 2D data sets for  $z$  and  $\phi$  in the space of  $(\Lambda, t)$  and each contains  $90001 \times 501$  datum. While training the network with data sets we randomly choose 9000 samples as a validation set, leaving the remaining 81001 samples for training. All computing results are based on Intel Core i7-7900X @3.30GHz and GeForce RTX 2060 with 1024 batch size and 32 filter size on Python 3.8.

An efficient learning depends on the design of network. To search for a suitable network, we compare the loss (after 400 epochs) and training time with several hidden-layers, as summarized in Table 1. In general as the increase of layer numbers the Mean-squared-error(MSE) loss becomes lower, however at the expense of a longer training time. To propose a low-expense method with high precision, we use *efficiency*(the last column in Table 1) as an indication for one network's compromised performance, which is defined by the training speed divided by the Tanh-type loss. It is clearly shown that a 7-layers model is the best one because of the maximal efficiency value  $\sim 9.92$ (bold). Also, we compare the results based on two different activation functions: Tanh and Sine. The Tanh-type function can bring a lower learning loss than the Sine function, which will

Layers	Loss for Tanh	Sine	Time(s)	Efficiency
5	0.0173	0.0192	7	8.26
<b>7</b>	<b>0.0112</b>	<b>0.0131</b>	<b>9</b>	<b>9.92</b>
9	0.0097	0.0102	11	9.37
11	0.0088	0.0092	15	7.58
13	0.0086	0.0089	20	5.81

**Table 1.** Comparison for training efficiencies under different number of hidden layers, activation functions and the average spending time for one epoch. Efficiency is given by the speed(=1/Time) divided by the Tanh's loss.

be considered in the calculation. In a practical training, we choose optimizer Adam for implementing the optimization<sup>38</sup>. In order to prevent over-fitting, the decay factor is 0.8, the minimum learning rate is  $5 \times 10^{-6}$  and the patience is 2 in the stage of Early-stopping and adaptive learning. The MSE loss function  $\mathcal{L}$  is defined by

$$\mathcal{L} = \frac{1}{N_{\Lambda}} \sum_{\Lambda} \sum_i^N \frac{(z(\Lambda, t_i) - g(\Lambda, t_i))^2}{N} \quad (9)$$

where  $z(\Lambda, t_i)$  is learning outcome *i.e.* the fractional population imbalance at  $t_i = \Delta t \times i (i \in [1, N])$  for each  $\Lambda$ ,  $g(\Lambda, t_i)$  is ground-truth from numerical solutions for each  $\Lambda$ .  $N$  is the length of arrays and  $N_{\Lambda}$  is the number of  $\Lambda$  learned in ResNet. Here  $N = 501$ ,  $\Delta t = 0.02$ ,  $N_{\Lambda} = 81001$ .

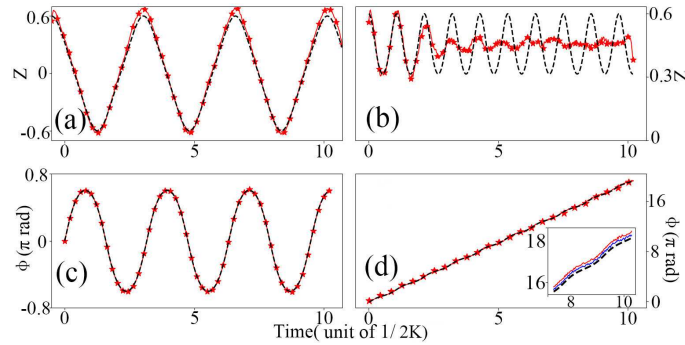


**Figure 2.** Direct learning of  $z(t)$ [(a-b)] and  $\phi(t)$ [(c-d)] marked by red stars. Numerical results are contrastively given by the black-dashed curves, as similar as the results in Fig.2(a-b). For (a,c)  $\Lambda = 6.2$ (BJJ regime),  $z(t)$  and  $\phi(t)$  solving from the two methods have a perfect agreement. As turning to the regime of MQST, *i.e.* (b,d)  $\Lambda = 13.4$ , only  $\phi(t)$  well agrees with the numerical prediction and  $z(t)$  exhibits a larger mismatch as time increases.

Figure 2 globally presents the direct learning outcome for the differences of population  $z(t)$  and phase  $\phi(t)$  in two regimes. As for the learning of phase difference our results well fit with the numerical predictions see (c-d). Note that when plotting (d) we do not constrain the range of  $\phi$ . So due to the linear increasing of  $\phi$  accompanied by a slight oscillation in the long-time regime, the number of layers(here we choose 7 hidden layers) becomes insufficient. As shown in the inset of (d), with the increase of layer numbers: *e.g.* 7 layers(red-solid), 9 layers(blue-solid), the learning outcome fits the numerical result(black-dashed) better. However, we find that the direct learning way can not work well for the  $z$ 's learning, especially in the MQST regime see (b). Because in this case atoms trapped in one well show a fast-oscillating behavior, leading to the breakdown of our thin single network that can not catch up with the change of  $z(t)$ . In the core of DL, such a rapid oscillation with small peak-peak amplitudes can not be easily trained by the limited database. Because the small loss in the whole process would cause gradient vanishing, making the learning process very inefficient.

To improve the learning quality, especially in the case of MQST where  $z(t)$  behaves as rapid oscillations with  $\langle z(t) \rangle \neq 0$ , we have to search for a new method. Since the periodicity of population dynamics is apparently seen, it is easy to decompose the function into frequency and amplitude components within one period. We can learn them individually based on the one-period's result, instead of a global optimization for all hyper-parameters. This new learning method will benefit from a low-expense network with fewer number of hidden layers as compared to the direct learning, if same accuracy is attainable. The modified network only needs a small receptive filed size which indeed reduces the number of kernel layers and its size. Before carrying out our method we have to verify the periodic feature of  $z(t)$ .

## Modified Learning

### Periodicity verification

Periodicity verification can facilitate the design of network in DL in this system. Compared to the traditional ways for that purpose such as Fourier Transform(FT)<sup>39</sup> and Auto-correlation Function(ACF)<sup>39</sup>, here we choose the method originating from the chaotic physics<sup>40,41</sup> which is called *Poincaré section* to determine  $z(t)$ 's periodicity since it is more visible. For an orbit in a two-dimension phase space, one could always select an appropriate hyperplane which should not contain or be tangent with this orbit. In general, if there are a fixed-point or fixed number of discrete points, the orbit should have a determined period<sup>42</sup>. Based on the nonlinearity of equation (4) we could use this method to determine the periodicity of dynamics.

In this double-well system, we choose  $\phi=0$  as a hyperplane in the BJJ regime and  $\phi=\pi$  in the MQST regime. We draw the points where the trajectory of  $(z - \dot{z})$  crosses this hyperplane. Specific examples are displayed in Supplementary Fig.S1 online in which the relations of  $(z - \phi)$ ,  $(z - \dot{z})$  and the Poincaré maps are given separately. When plotting the Poincaré maps it is clearly shown that only some discrete points exist confirming the periodic character of  $z(t)$ .

### Frequency learning

A complete simulation for the frequency  $f$  as a function of  $\Lambda$  has been numerically solved in Fig.1d in which the critical frequency at  $\Lambda = \Lambda_c$  is fixed to be 0.1. When turning to the problem of solving an one-dimensional array of data, *e.g.* learning frequency of fractional population difference  $z(t)$ , ResNet is not the best choice since it typically suits for extracting the feature of a two-dimensional array<sup>43,44</sup>, such as the learning of  $z(\Lambda, t)$ ,  $\phi(\Lambda, t)$  in Direct Learning. Here we introduce a modified Recurrent Neural network which is so-called "Long Short-Term Memory"(LSTM) for that purpose<sup>23</sup>. This method has been applied for studying knot types of polymer conformations<sup>7</sup> and phase-modulation stabilization in quantum key distribution<sup>46</sup>. Because it performs pretty well in time-series fitting and prediction. Although its weakness lies in a requirement of more time to train in contrast to the case of using ResNet if the same number of layers are used. Luckily it performs better in preventing from gradient vanishing and exploding in the long-range-series training.

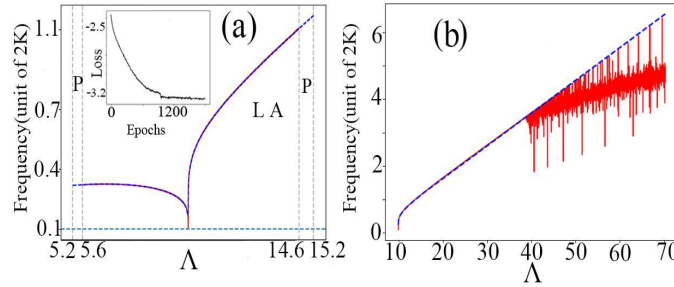


**Figure 3.** (a) Learning of frequency in the original learning area(LA):  $\Lambda \in [5.6, 14.6]$ . The prediction results denoted by “P” are given in the area of  $\Lambda \in [5.2, 5.6]$  and  $[14.6, 15.2]$ . Our LSTM learning outcomes(blue-dashed) perfectly agree with the numerical results (red-solid). Inset shows the corresponding MSE loss  $\mathcal{L}$  in the form of logarithmic function versus epochs. (b) Frequency learning in the case of an extensive range of  $\Lambda \in [10, 70]$ . Same linetypes are used.

The results of learning frequency are presented in Supplementary Table S1 online and Figure 3. Table S1 compares the MSEs under different hidden layers by using various activation functions: Tanh, Sine and Mixture. For obtaining an optimal network we also consider the time expense, leading to an efficiency that quantitatively stands for the learning performance. We find only 6 layers(bold) is sufficient for learning. Here we also use Early-stopping to avoid over-fitting. RMSprop is chosen as a new optimizer in LSTM network. The original training area is the same as in direct learning *i.e.*  $\Lambda \in [5.6, 14.6]$  but a wider range of  $\Lambda \in [5.2, 15.2]$  is given based on the prediction of LSTM. A good agreement with the numerical results is confirmed in Fig.3a except for the critical point  $\Lambda_c = 10$  since the network treats it as an outlier(singularity) due to the discontinuity. Inset plots the change of MSE loss  $\mathcal{L}$  that has been reduced to be much smaller than 0.001 when the epoch grows, which means the way of LSTM is helpful for an individual frequency learning in the training process.

Remarkably, with the increase of  $\Lambda$  (*i.e.* the oscillating frequency) the numerical method becomes inefficient to give accurate results due to the calculation precision limited by a sampling interval  $\Delta t = 0.02$ . Reducing  $\Delta t$  could enhance the precision yet adding to the cost. So a bigger mismatch will appear between the numerically-estimated values and the real numbers when  $\Lambda \gtrsim 40$ , see the red-solid curve in Fig.3b. However the LSTM network can preserve a robust prediction for higher frequency values (blue-dashed) within a broader range of  $\Lambda \in [10, 70]$ , although the initial data set based on  $\Lambda \in [5.6, 14.6]$  and  $\Delta t = 0.02$  are unchanged in the learning. So the LSTM network could be expected to be suited for solving the fast-oscillating behavior even if the sampling points are inadequate or in low-frequency regime.

## Modified network

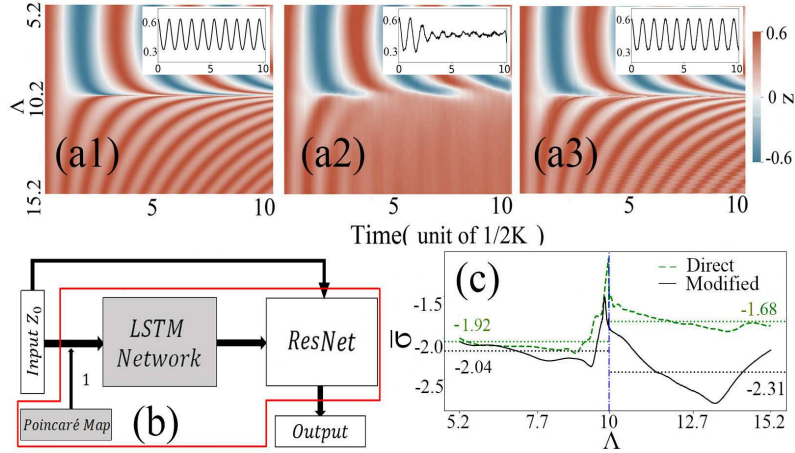


**Figure 4.** Representation of the population dynamics  $z$  in the space of  $(t, \Lambda)$  under (a1) numerical simulation, (a2) direct learning, (a3) modified learning. Insets show the population dynamics  $z(t)$  for  $\Lambda = 13.4$  using different methods. (b) The procedure of our modified network by sequentially combining LSTM and ResNet. (c) Comparison of relative errors in logarithm form between direct learning (green dashed) and modified learning (black solid). Average values (dashed lines) are also given separately.

A new modified network can be reconstructed by taking account into the ability of LSTM in learning frequency. Thinner networks can only capture limited local information with a small receptive field size<sup>47</sup>. Therefore, our method makes it possible to produce a hybrid network with LSTM and ResNet that generates the whole population dynamics within a small receptive field size. In this hybrid learning network as shown in Fig.4b, the former LSTM network is used for frequency learning by the way of Poincaré map at the first stage. Additionally, the ResNet treats as a core network globally generating the complete fractional population difference dynamics  $z(t, \Lambda)$ . For ResNet learning, we also use the MSE loss function  $\mathcal{L}$  [equation (9)], but with  $z(t_i)$ ,  $N$ ,  $g(t_i)$  the parameters obtained after implementing the LSTM network. In the core of our procedure [see red box in Fig.4b], we use the Poincaré maps and LSTM network integrated to transmit extra information to ResNet in which the way of Poincaré map can improve the learning fidelity via periodicity verification before learning.

Figure 4(a1-a3) globally present the results of  $z(t, \Lambda)$  under numerical simulation, direct learning as well as our modified network learning. A special case of  $z(t, 13.4)$  is shown in Insets accordingly. Clearly the direct learning method gives to poor results in the MQST regime as compared to the numerical calculation because of the strong oscillation. The direct learning only contains single ResNet that is insufficient for grasping the fast-oscillating behavior. However a significant improvement has been identified if two blocks of Poincaré map and LSTM network are added in the procedure diagram. A quantitative comparison between direct and modified learning results uses the mean relative error

$$\bar{\sigma}(\Lambda) = \frac{1}{N} \sum_i^N \frac{|z(t_i, \Lambda) - g(t_i, \Lambda)|}{0.1 + |g(t_i, \Lambda)|} \quad (10)$$

where  $z(t_i, \Lambda)$  and  $g(t_i, \Lambda)$  obtained from the network training and the numerical ground-truth, are also  $\Lambda$ -dependent. Here 0.1 serves as an arbitrary small quantity to overcome the divergency. This error represents the derivation between learning outcome and numerical ground-truth, *i.e.* the infidelity of learning. In the BJJ region two learning ways lead to comparable errors ( $10^{-1.92}$  and  $10^{-2.04}$ ), confirming the efficiency of learning methods. However as turning to the MQST region the modified learning apparently causes the reduction of mean relative error from  $10^{-1.68}$  to  $10^{-2.31}$ , which extremely increases the capability of network in learning a fast-oscillating dynamics, leading to a high-fidelity learning method.

By now, the hybrid system that contains a sequential LSTM and ResNet networks, can provide an improved learning quality for the population dynamics, especially in the MQST regime. While we also note that, two networks must be trained independently which suffer from a long-time expense. A typical time expense is 34 seconds for one-epoch training. To overcome this weakness we propose an integrated network by combining LSTM and ResNet together with the help of feedback mechanism. This new learning method can further accelerate the training speed, saving the time by 15% or more in an one-epoch training.

## Integrated Learning

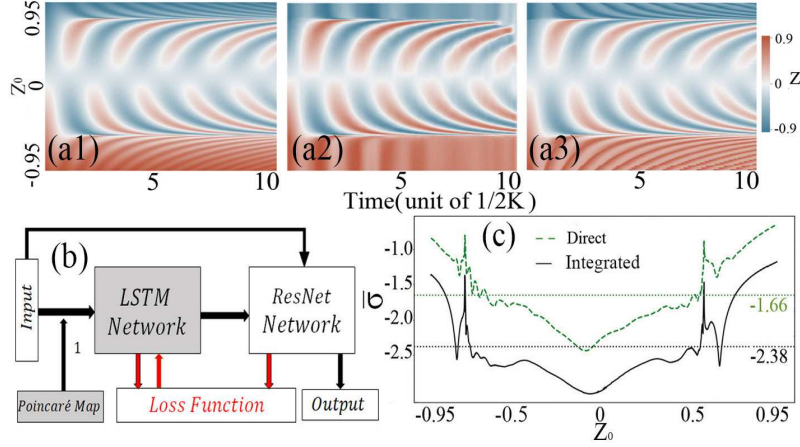


**Figure 5.** (a1-a3) Representation of the population dynamics  $z(t)$  in space of  $(t, z_0)$  using the methods of numerical simulation, direct learning and integrated learning respectively. (b) Integrated learning procedure. The frequency learning by LSTM is facilitated due to the feedback mechanism from ResNet learning (red arrows). (c) Relative errors  $\bar{\sigma}$  in logarithmic form versus the initial imbalanced population  $z_0 = z(t=0)$  from direct learning and integrated learning.

A universal study for the population dynamics in an asymmetric double-well is performed. Motivated by Ref.<sup>48</sup> it is possible to utilize the feedback of loss from ResNet learning to train the former LSTM network, instead of a direct frequency learning by it, in order to accelerate the learning speed. The role of LSTM is providing the frequency information for the next ResNet learning due to the thin and small convolutional network of Resnet. Similarly, the frequency periodicity verification is carried out by using *Poincaré section* as shown in Supplementary Fig. S2. If the loss function of ResNet can be treated as an indicator for the LSTM network's learning it would largely improve its learning efficiency. Because the MSE loss function defines the deviation between final outcome and the ground-truth value.

In the practical training we follow the procedure diagram in Fig.5b. It differs from the modified learning mainly owing to the use of a new loss function  $\mathcal{L}_{\mathcal{G}}$ , which can be expressed as

$$\mathcal{L}_{\mathcal{G}} = \mathcal{L} - k \sum_{z_0}^{N_{z_0}^*} \frac{(f(z_0) - f_g(z_0))^2}{N_{z_0}^*}, \quad (11)$$

where  $k$  is a weight factor and  $N_{z_0}^*$  denotes the partial data number to train LSTM. To show the learning for an asymmetric well we use the initial population difference  $z_0$  as a tunable parameter, instead of  $\Lambda$ . The first term  $\mathcal{L}$  standing for the loss estimation in single ResNet learning, takes a similar form like equation. (9). The second term serves as an auxiliary for showing the deviation of real frequency  $f$  from the ground-truth  $f_g$  with respect to each  $z_0$ . Therefore the ResNet learning can offer an efficient feedback for the frequency learning within the LSTM network. Our scheme follows the procedure in Fig.5b. In order to minimize  $\mathcal{L}_{\mathcal{G}}$  as well as to speed up the convergence of this integrated network, we perform an individual training for two networks at initial steps. After that we fix the ResNet and let the LSTM being trained for steps to minimize  $\mathcal{L}_{\mathcal{G}}$  accompanied by generating an array of frequency for each  $z_0$ . In addition we also simultaneously train ResNet to reduce the value of  $\mathcal{L}$ . Based on our practical training, we set four steps for LSTM's training and five steps for ResNet in each iteration, the weight factor is  $k = 1.4$ .

The integrated learning bases on the fractional population difference  $z(t, z_0)$  in an asymmetric double-well system where  $\gamma = 1.0$  is assumed. Here we set  $\Lambda = 8$  and treat  $z_0 = z(t=0) \in [-0.95, 0.95]$  as a variable. After implementing a periodic verification of  $z$  with the method of Poincaré maps (see in Supplementary Fig. S2 online) we do the learning following the procedure of Fig.5b. Figure 5(a1-a3) plot similar results as Fig.4(a1-a3) yet within the  $(t, z_0)$  space. Clearly the results obtained from the integrated learning in (a3) also get a better fidelity as compared to that from direct learning [(a2)], leading to a deeply reduced relative error  $\bar{\sigma}$  as presented in Fig.5c. Note that in the integrated learning we only compute partial data for estimating the frequency *i.e.*  $N_{z_0}^* = 1201$  (the total number is  $N_{z_0} = 7601$ ), benefiting from the feedback mechanism. While it can reduce the relative error *i.e.* the infidelity from  $10^{-1.66}$  to  $10^{-2.38}$  on average by using an integrated neural network.

Method	Training(s)	Generation(ms)	Parameter $\Lambda$	Error	Efficiency
Runge-Kutta	-	1.15	[5.6, 14.6]	-	-
Direct Learning	20	3.98	[5.2, 10]	0.0123	4.07
	20	3.98	[10, 15.2]	0.0209	2.39
Modified Learning	34	5.37	[5.2, 15.2]	0.0066	4.46
Integrated Learning	29	5.19	[5.2, 15.2]	0.0063	<b>5.47</b>

**Table 2.** In a symmetric double-well system, time expense required for training and generating data  $z(t, \Lambda)$  in one epoch using four methods. The training parameter range, the relative error and learning efficiency are comparably given for same training layers. The total layer number is 13 including 6 layers for LSTM and 7 layers for ResNet. For direct learning we use a 13-layer ResNet.

## Discussion and Conclusion

Before ending we have to compare the efficiency of three deep learning methods. Given the original numerical data generated by solving theoretical equations [equation (4)] we compare the learning results in Table 2. When the original data set for  $z(t)$  is created under the parameter range of  $\Lambda \in [5.6, 14.6]$ , various learning methods can study their characters by training. Although the training process costs much longer time than generation it is possible to predict unknown results beyond the given parameter range. Note that here a direct learning with a 13-layer ResNet fails to fit the real population dynamics on the MQST regime, leading to a poor efficiency  $\sim 2.39$ (the infidelity is 0.0209). However, accompanied by an auxiliary LSTM network that provides a periodicity certification of frequency, this hybrid network(modified learning and integrated learning) can show a significant improvement in increasing the learning efficiency, reaching as high as  $\sim 5.47$ (the final infidelity obtained for  $z(t)$  is far smaller than 0.01) for the integrated learning. Besides the hybrid network can provide a precise learning in both BJJ and MQST regimes, which can even make predictions about data within an unknown parameter range that is not given by the original data set. For learning in a higher-frequency regime such as MQST where the Runge-Kutta method becomes inaccessible due to the finite time interval  $\Delta t$ , our LSTM network can still robustly make predictions about the higher frequency values with the same data set.

In conclusion we have developed a hybrid “*LSTM+ResNet*” network to revisit the problem of time-dependent population and phase dynamics in a double-well optical potential. The fast-oscillating behavior of imbalanced population on the MQST regime, makes the traditional direct learning inaccessible. However we propose a novel DL method that integrates LSTM and ResNet networks, enabling a strong promotion to the learning efficiency. The LSTM also represents a robust prediction for higher frequencies. This hybrid network not only performs better with a high precision and a very low relative error (the final infidelity obtained for the fractional population difference)  $\sim 0.006$ , but also could be used as a verification for the accuracy of theory. Most importantly, it can show a predictable power for the fast-oscillation characters which are far beyond the original data sets given by the numerical simulation. This prediction capability of method could find more applications in other physical systems which are lack of sufficient parameters restrained by the experimental conditions or real expenses. More practical applications of the new hybrid network will be discussed in the future.

## Methods

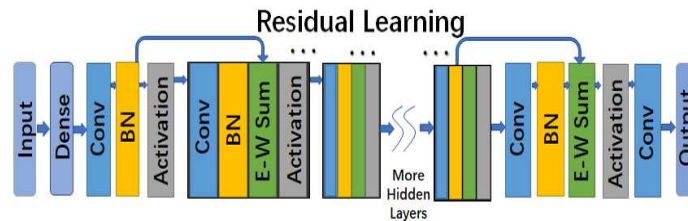


**Figure 6.** Schematic diagram for ResNet network involving a series of identically-distributed one-dimension convolutional (Conv) layers and batch normalization (BN) layers. At each convolutional layer it has a dilation rate except the first and the last layers. Different from the original convolutional NN scheme, arrows acting on Element-wise sum layers(E-W sum) can preserve the former hidden layer’s information which facilitate the performance of DL.

Structure of our residual network is shown by a series of blocks in Fig. 6. The filter kernel serving as a central element in

learning process, should be carefully chosen. We use filter kernels to scan matrices which enables the feature extraction from objects. By element-wisely multiplying matrices and filter kernels, machine can well learn the input features. However, with deeper networks, a traditional convolutional NN becomes more difficult to train, since we may face the problem of gradient vanishing or gradient exploding, which lead to poor performance on DL. Hence, we choose a residual network (or so-called *ResNet*) to solve this problem. An element-wise sum in the ResNet labeled by arrows in Fig. 6, will prevent the loss of information from passing through deep networks, and also avoid the vanishing of gradient by adding the former input with present hidden layer's output. This simple process preserves the former information which means it increases the volume of data handled by the next layer. The detail of this technology can be seen in reference<sup>24</sup>. To be more specific, arrows linking the BN layer and the E-W sum layer in Fig.6 point to the process of residual learning.

From physical review, we are more interested in training or generating useful information within a "black box" (the red frame in Fig.4b) if the input is determined. Although training a high-performance network needs a lot of expense yet it may enable a robust prediction for the unknown results in a short-time period, especially while dealing with a complex system in the absence of analytical solutions. Our motivation is building an efficient learning tool which can bridge the results from original numerical simulation and unknown prospective result based on the given input parameters, facilitating an easy and robust simulation for solving complex physical problems.

## References

1. I. A. Luchnikov, S. V. Vintskevich, D. A. Grigoriev, and S. N. Filippov. Machine learning non-markovian quantum dynamics. *Phys. Rev. Lett.*, 124:140502, Apr 2020.
2. XW Liu, GJ Zhang, J Li, GL Shi, MY Zhou, BQ Huang, YJ Tang, XH Song, and WF Yang. Deep learning for Feynman's path integral in strong-field time-dependent dynamics. *Phys. Rev. Lett.*, 124:113202, Mar 2020.
3. Giuseppe Carleo and Matthias Troyer. Solving the quantum many-body problem with artificial neural networks. *Science*, 355(6325):602, 2017.
4. Alexander Hentschel and Barry C. Sanders. Machine learning for precise quantum measurement. *Phys. Rev. Lett.*, 104:063603, Feb 2010.
5. PF Zhang, HT Shen, and Hui Zhai. Machine learning topological invariants with neural networks. *Phys. Rev. Lett.*, 120:066401, Feb 2018.
6. G. Torlai, G. Mazzola, J. Carrasquilla, M. Troyer, R. Melko, and G. Carleo. Neural-network quantum state tomography. *Nature Physics*, 14:447, 2018.
7. Kelvin Ch'ng, Juan Carrasquilla, Roger G. Melko, and Ehsan Khatami. Machine learning phases of strongly correlated fermions. *Phys. Rev. X*, 7:031038, Aug 2017.
8. Evert.P.L. van Nieuwenburg, YH. Liu, and Sebastian D. Huber. Learning phase transitions by confusion. *Nature Physics*, 14:435, 2017.
9. J. Carrasquilla and R. Melko. Machine learning phases of matter. *Nature Physics*, 13:431, 2017.
10. SR Lu, LM Duan, and DL Deng. Quantum adversarial machine learning. *Phys. Rev. Research*, 2:033212, Aug 2020.
11. XL. Ouyang, XZ. Huang, YK. Wu, WG. Zhang, X. Wang, HL. Zhang, L. He, XY. Chang, and LM. Duan. Experimental demonstration of quantum-enhanced machine learning in a nitrogen-vacancy-center system. *Phys. Rev. A*, 101:012307, Jan 2020.
12. Vedran Dunjko, Jacob M. Taylor, and Hans J. Briegel. Quantum-enhanced machine learning. *Phys. Rev. Lett.*, 117:130501, Sep 2016.
13. G. Cybenko. Approximation by superpositions of a sigmoidal function. *Mathematics of Control, Signals and Systems*, 2(4):303, 1989.
14. LJ. Ba and R. Caruana. Do deep nets really need to be deep? *Advances in neural information processing systems*, 3:2654, 2014.
15. Domingos S. P. Salazar. Nonequilibrium thermodynamics of restricted Boltzmann machines. *Phys. Rev. E*, 96:022131, Aug 2017.
16. Geoffrey Hinton, Simon Osindero, and Yee-Whye Teh. A fast learning algorithm for deep belief nets. *Neural computation*, 18:1527, 08 2006.
17. Y Lecun and L Bottou. Gradient-based learning applied to document recognition. *Proceedings of the IEEE*, 86(11):2278, 1998.

18. Mohamed Hibat-Allah, Martin Ganahl, Lauren E. Hayward, Roger G. Melko, and Juan Carrasquilla. Recurrent neural network wave functions. *Phys. Rev. Research*, 2:023358, Jun 2020.
19. Ana Diaz Rivero and Cora Dvorkin. Direct detection of dark matter substructure in strong lens images with convolutional neural networks. *Phys. Rev. D*, 101:023515, Jan 2020.
20. Mahesh Kumar Mulimani, Jaya Kumar Alageshan, and Rahul Pandit. Deep-learning-assisted detection and termination of spiral and broken-spiral waves in mathematical models for cardiac tissue. *Phys. Rev. Research*, 2:023155, May 2020.
21. Viktor Novičenko, Julius Ruseckas, and Egidijus Anisimovas. Quantum dynamics in potentials with fast spatial oscillations. *Phys. Rev. A*, 99:043608, Apr 2019.
22. C. E. Shannon. Communication in the presence of noise. *Proceedings of the IRE*, 37(1):10–21, 1949.
23. S Hochreiter and J Schmidhuber. Long short-term memory. *Neural Computation*, 9(8):1735, 1997.
24. K. He, X. Zhang, S. Ren, and J. Sun. Deep residual learning for image recognition. *2016 IEEE Conference on Computer Vision and Pattern Recognition (CVPR)*, page 770, 2016.
25. X Liang, S Liu, Y Li, and YS Zhang. Generation of bose-einstein condensates' ground state through machine learning. *Scientific Reports*, 8, 11 2018.
26. G. Valtolina, A. Burchianti, A. Amico, E. Neri, and Giacomo Roati. Josephson effect in fermionic superfluids across the BEC-BCS crossover. *Science*, 350(6267), 2015.
27. J. Dobrzyniecki and T Sowiński. Effective two-mode description of a few ultra-cold bosons in a double-well potential. *Physics Letters A*, 382(6):394, 2018.
28. A.Smerzi, S.Fantoni, S.Giovanazzi, and S.R.Shenoy. Quantum coherent atomic tunneling between two trapped Bose-Einstein condensates. *Phys. Rev. Lett.*, 79:4950, Dec 1997.
29. G. Spagnolli, G. Semeghini, L. Masi, G. Ferioli, A. Trenkwalder, S. Coop, M. Landini, L. Pezzè, G. Modugno, M. Inguscio, A. Smerzi, and M. Fattori. Crossing over from attractive to repulsive interactions in a tunneling bosonic Josephson junction. *Phys. Rev. Lett.*, 118:230403, Jun 2017.
30. Marine Pigneur and Jörg Schmiedmayer. Analytical pendulum model for a bosonic Josephson junction. *Phys. Rev. A*, 98:063632, Dec 2018.
31. Sofía Martínez-Garaot, Giulio Pettini, and Michele Modugno. Nonlinear mixing of Bogoliubov modes in a bosonic Josephson junction. *Phys. Rev. A*, 98:043624, Oct 2018.
32. M. Jääskeläinen and P. Meystre. Dynamics of Bose-Einstein condensates in double-well potentials. *Phys. Rev. A*, 71:043603, Apr 2005.
33. N. R. Thomas, A. C. Wilson, and C. J. Foot. Double-well magnetic trap for Bose-Einstein condensates. *Phys. Rev. A*, 65:063406, Jun 2002.
34. R. W. Spekkens and J. E. Sipe. Spatial fragmentation of a Bose-Einstein condensate in a double-well potential. *Phys. Rev. A*, 59:3868, May 1999.
35. H. M. Cataldo and D. M. Jezek. Dynamics in asymmetric double-well condensates. *Phys. Rev. A*, 90:043610, Oct 2014.
36. Y. Shin, M. Saba, T. A. Pasquini, W. Ketterle, D. E. Pritchard, and A. E. Leanhardt. Atom interferometry with Bose-Einstein condensates in a double-well potential. *Phys. Rev. Lett.*, 92:050405, Feb 2004.
37. Michael Albiez, Rudolf Gati, Jonas Fölling, Stefan Hunsmann, Matteo Cristiani, and Markus K. Oberthaler. Direct observation of tunneling and nonlinear self-trapping in a single bosonic Josephson junction. *Phys. Rev. Lett.*, 95:010402, Jun 2005.
38. Diederik Kingma and Jimmy Ba. Adam: A method for stochastic optimization. *Computer Science*, 2014.
39. Scargle and D. Jeffrey. Studies in astronomical time series analysis. iii - Fourier transforms, autocorrelation functions, and cross-correlation functions of unevenly spaced data. *Astrophysical Journal*, 343:874, 1989.
40. D. O. Pushkin, D. E. Melnikov, and V. M. Shevtsova. Ordering of small particles in one-dimensional coherent structures by time-periodic flows. *Phys. Rev. Lett.*, 106:234501, Jun 2011.
41. Fatemeh Tajik, Mehdi Sedighi, Mohammad Khorrani, Amir Ali Masoudi, and George Palasantzas. Chaotic behavior in Casimir oscillators: A case study for phase-change materials. *Phys. Rev. E*, 96:042215, Oct 2017.
42. ZH. Liu. *Chaotic dynamics foundation and its application in brain functions*. Science Press, 2018.

43. Stavros Efthymiou, Matthew J. S. Beach, and Roger G. Melko. Super-resolving the Ising model with convolutional neural networks. *Phys. Rev. B*, 99:075113, Feb 2019.
44. ZM Li, SB Wu, J Gao, H Zhou, ZQ Yan, RJ Ren, SY Yin, and XM Jin. Fast correlated-photon imaging enhanced by deep learning. *Optica*, 8(3):323, Mar 2021.
45. HG Chen, XH He, QZ Teng, Raymond E. Sheriff, JX Feng, and SH Xiong. Super-resolution of real-world rock micro-computed tomography images using cycle-consistent generative adversarial networks. *Phys. Rev. E*, 101:023305, Feb 2020.
46. JY Liu, HJ Ding, ChM Zhang, SP Xie, and Q Wang. Practical phase-modulation stabilization in quantum key distribution via machine learning. *Phys. Rev. Applied*, 12:014059, Jul 2019.
47. F. Milletari, N. Navab, and S. Ahmadi. V-net: Fully convolutional neural networks for volumetric medical image segmentation. In *2016 Fourth International Conference on 3D Vision (3DV)*, pages 565–571, 2016.
48. L. Xie, Q. Yu, Y. Zhou, Y. Wang, E. K. Fishman, and A. L. Yuille. Recurrent saliency transformation network for tiny target segmentation in abdominal CT scans. *IEEE Transactions on Medical Imaging*, 39(2):514, 2020.

## Acknowledgements

This work was supported by the NSFC under Grants No.11474094 and No.11104076, by the Science and Technology Commission of Shanghai Municipality under Grant No.18ZR1412800

## Additional information

**Competing interests** The authors declare no competing interests.